NUKLEONIKA 2013;58(3):351–357

ORIGINAL PAPER

Interaction of diatomic molecules with nickel ions inside the channels of high silica zeolites – an EPR and DFT study

Tomasz Mazur, Katarzyna Podolska, Piotr Pietrzyk, Zbigniew Sojka

Abstract. Interaction of CO, NO, and O_2 diatomics with Ni^{II} and Ni^{I} ions dispersed in ZSM-5 zeolite was investigated by electron paramagnetic resonance (EPR) spectroscopy and density functional theory (DFT) modelling. The resulting adducts Ni^{I}-CO, Ni^{II}-NO, and Ni^{I}-O_2 were identified based on *g*-tensor parameters, obtained by computer fitting of the powder EPR spectra, and next ascertained by parallel relativistic DFT calculations of the corresponding *g*-tensor values. The structures of the Ni^{I}-CO, Ni^{II}-NO, and Ni^{I}-O_2 complexes were obtained by geometry optimization with the Kohn-Sham method. Binding of the diatomics was discussed in terms of the spin-pairing and electron density transfer events. Interaction of CO with Ni^{I} cations led to the pronounced change in the coordination and electronic structure of the Ni^{I} center, however, no redox processes were observed in agreement with the "innocent" nature of CO as a ligand. On the contrary, strong electron and spin density redistribution was observed upon NO and O_2 interaction ("non-innocent ligands") leading to the formation of the bound nitrosonium $NO^{\delta+}$ and superoxo O_2^- species, respectively.

Key words: electron paramagnetic resonance (EPR) spectroscopy • *g*-tensor • nickel • zeolite • small molecule activation

T. Mazur, K. Podolska, P. Pietrzyk✉, Z. Sojka
Faculty of Chemistry,
Jagiellonian University,
3 R. Ingardena Str., 30-060 Kraków, Poland,
Tel.: +48 12 663 2224, Fax: +48 12 634 0515,
E-mail: pietrzyk@chemia.uj.edu.pl

Received: 17 August 2012
Accepted: 15 January 2013

Introduction

Binding and activation of small gas-phase diatomic molecules (XY) such as H_2, CO, N_2, NO, O_2 by transition-metal ions (TMI) involves the most elementary chemical processes at the electronic level [19]. Among them charge and spin density flows within the TMI-XY moiety depend critically on the nature of the coordinated diatomics, and can lead either to redox ("non-innocent ligand") or non-redox ligation ("innocent ligands"). Typical examples of such ligands are carbon monoxide (innocent ligands) and dioxygen or nitric oxide (non-innocent ligands). These important molecules are implicated in many catalytic and enzymatic processes for which TMI usually constitute the active centres exemplified, e.g., by metallozeolites or prosthetic groups of metalloproteins and enzymes. In this context, nickel ions are the cores of many catalysts [6, 8, 11] and enzymes [1, 5] where CO, NO, and O_2 play the role of important reactants.

It has been recently shown that reactive binding of the diatomics triggers the redox cycles of the metal centres stabilized inside the channels of porous materials. For instance, 2-electron Co^{II}/Co^{0} redox cycle in ZSM-5 zeolite is initiated by binding of NO [13], whereas 1-electron Ni^{II}/Ni^{I} cycle is observed upon interaction with NO [11, 16] and O_2 [8]. The concomitant changes of the metal and ligand oxidation state in connection with the paramagnetic nature of the NO, O_2 ligands and the $Ni^{I/II}$ active sites result in a profound transfer of the spin density upon ligation, which can be experimentally followed by means of electron paramagnetic resonance (EPR)

spectroscopy. Apart from *g*-tensor anisotropy, helpful in deducing the symmetry of the resultant adducts [9], hyperfine coupling constants (for labelled molecules ^{13}CO, ^{14}NO, $^{17}O_2$) or quadrupole interaction parameters (for ^{14}N $I = 1$, ^{17}O $I = 5/2$) can be obtained either by continuous-wave or pulsed measurements, depending on their magnitudes [14].

The aim of this work is to investigate the binding of the topical CO, NO, and O_2 molecules by nickel(II) and nickel(I) active centres dispersed in the high-silica zeolites (ZSM-5, BEA). Experimental parameters of the resulting complexes were obtained by CW-EPR spectroscopy. Attribution of the observed EPR signals and identification of the adsorption geometries were guided by relativistic density functional theory (DFT) calculations of the magnetic parameters [12] for model structures mimicking the real complexes.

Experimental and computational methods

Nickel-exchanged zeolites were obtained by a standard ion exchange method using the ZSM-5 zeolite (Zeolyst, Inc.) with Si/Al = 15 and BEA zeolite (Tricat) with Si/Al = 12. Chemical analysis by means of the atomic absorption spectroscopy (AAS) method revealed the nickel loading of 0.75 and 2.04 wt.%, respectively. Prior to the spectroscopic measurements, the samples were activated in vacuum (10^{-5} mbar at 773 K for 2 h) and either reacted directly with CO, NO, O_2 (1–10 mbar) or reduced with CO (673 K), followed by evacuation and then adsorption of the gas-phase reactants. CW-EPR spectra were recorded with a Bruker ELEXSYS-580 X-band spectrometer with the 100 kHz field modulation, equipped with a nitrogen variable temperature unit. The microwave power of 1–100 mW and the modulation amplitude of 0.2–0.5 mT were applied. For computer simulation of the powder spectra, the EPRsim32 program was used [17].

DFT calculations and geometry optimization were carried out with ADF software utilizing BP exchange-correlation functional and TZP basis set [18]. The EPR parameters were calculated with ORCA program [3] for which variety of the exchange-correlation functionals and basis sets were tested. Scalar zeroth order regular approximation (ZORA) corrections to the electronic structure were applied. The *g*-tensor parameters were calculated as the second order properties with the spin-orbit contributions assessed from spin-orbit mean field (SOMF) approximation [7].

Results and discussion

Electronic structure of CO, NO and O_2 molecules

Preliminary insight into the electronic structure of the investigated diatomics was gained by DFT calculations. Characteristic feature of a CO molecule ($^1\Sigma$) is a strongly localized σ-type highest occupied molecular orbital (HOMO) of a slightly antibonding nature (Fig. 1). Due to a pronounced lobe of the lone electron pair centered at carbon atom, CO as a ligand predominantly exhibits η^1-C binding geometry, and it is also responsible for its Lewis basic properties in reactions with TMI. Because of the strong antibonding nature of the lowest unoccupied molecular orbital (LUMO) and a large HOMO-LUMO gap (ΔE = 7.02 eV), CO is the non-redox ligand, avoiding depletion of spin density from TMI upon coordination. Instead, its ligation often leads to a strong rehybridization of *d*-electron states [9, 10]. At the same time, the presence of the empty π* states provides a pathway for efficient overlap between CO and TMI orbitals, making the energy difference between the relevant *d*-hybrids relatively small. As a consequence, *g*-tensor anisotropy increases as will be shown below.

The NO molecule is the $^2\Pi_{1/2}$ radical with the unpaired electron density equally smeared out between two orthogonal π*(2*p*) states. In DFT calculations this situation is reflected by 0.5 occupation numbers of both α-HOMO states (Fig. 1). Upon interaction with TMI, the cylindrical symmetry is removed making one of the

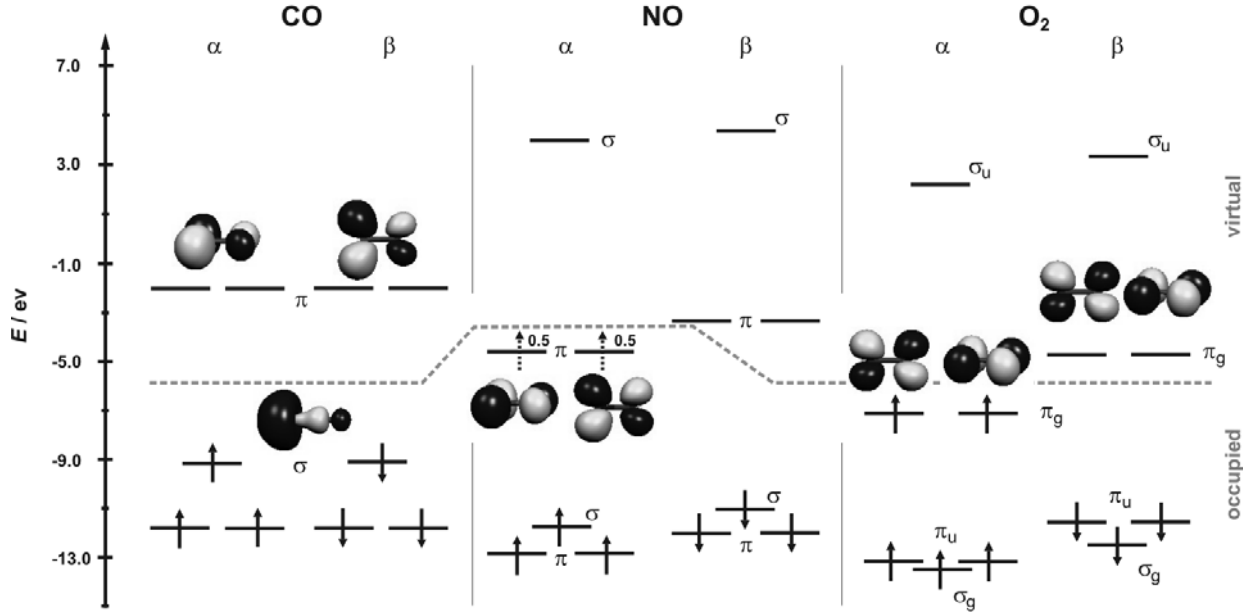

Fig. 1. Kohn-Sham orbital diagrams for CO, NO, and O_2 diatomic molecules. One-electron orbital levels in spin resolution and contours of the frontier spin-orbitals are shown. In the NO diagram, 0.5 indicates fractional occupation of the degenerate π* states.

α-HOMO lower in energy and allowing its integer population. However, because of the highest energy level of α-HOMO (E_{HOMO} = –4.60 eV) among the investigated diatomics, NO molecule exhibits versatile electron transfer abilities leading to two limiting nitrosonium (NO^+) or nitrozide (NO^-) species, depending on the energy of the *d*-states of the interacting TMI.

The O_2 molecule exhibits high-spin ground state ($^3\Sigma_g^-$) with two orthogonal singly-occupied $\pi_g^*(2p)$ α-HOMO shown in Fig. 1. Despite its open-shell nature, dioxygen exhibits a relatively low reactivity toward organic molecules. This feature is related to the triplet--singlet spin barrier, which can be circumvented upon interaction with TMI. The first step in activation of the dioxygen molecule consists of electron transfer from metal to ligand, to form a metal-superoxo (1-electron reduction) or peroxo (2-electron reduction) species. This is possible because of the low-laying β-LUMO orbitals, which can accommodate additional electron (spin) density due to high electronegativity of dioxygen. Both side-on (η^1) and end-on (η^2) modes of O_2 coordination are possible.

Binding and activation of CO

The EPR spectra of the CO, NO and O_2 adducts with Ni-exchanged zeolites can be accounted for with the following spin-Hamiltonian

$$H = \sum_i \mu_B \boldsymbol{B}^T \boldsymbol{g}_i \boldsymbol{S}_i + \sum_{i,k} \boldsymbol{I}_k^T \boldsymbol{A}_k \boldsymbol{S}_i \quad (1)$$

where the first part reflects the electron Zeeman term, whereas the second one the hyperfine interaction term. In the spectra discussed below only the anisotropy of Zeeman interaction was observed since no spin-labelled adsorbates were used.

Activation of diamagnetic CO molecule was investigated on the samples containing paramagnetic (reduced) state of nickel. Monovalent nickel (S = 1/2) was generated by mild reduction of the thermally activated Ni^{II}ZSM-5 zeolite by CO. Reduction was possible owing to the formation of dinuclear nickel-oxo species, Ni^{II}-O-Ni^{II}, in the course of the ionic exchange. They are easily reduced by CO according to the following reaction

$$Ni^{II}\text{-O-}Ni^{II} + CO = 2Ni^{I} + CO_2 \quad (2)$$

leading to generation of the isolated Ni^I centres. EPR spectra before and after reduction in CO are shown in Fig. 2. The parent zeolite contains both bare Ni^{II} (S =

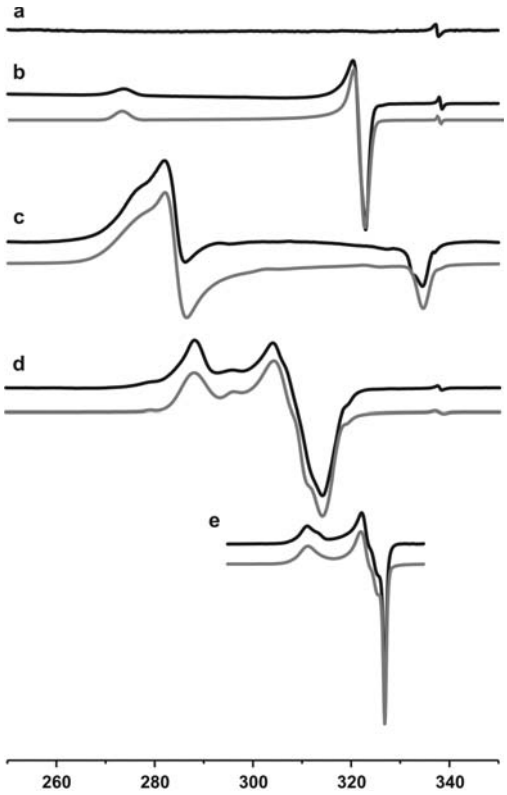

Fig. 2. X-band EPR spectra recorded at 77 K of (a) parent activated Ni^{II}ZSM-5 sample, (b) reduced in CO and evacuated Ni^IZSM-5 sample, (c) sorption of CO (p < 1 mbar) on the Ni^IZSM-5, (d) 5 mbar of NO adsorbed on the Ni^{II}ZSM-5, and (e) 1 mbar of O_2 adsorbed on the Ni^IZSM-5. Experimental spectra are shown in black, simulated spectra, in grey. Weak signal at g ~ 2.0 (333 mT) is due to thermally induced defects of zeolite framework.

1) and dimer Ni^{II}-O-Ni^{II} centres. None of them could be observed in X-band (Fig. 2a) because of the high zero field splitting and antiferromagnetic coupling J = –33.27 cm^{-1} (calculated with broken-symmetry method), respectively. On the contrary, the reduced Ni^I gave a clear nearly axial signal ($g_{xx,yy}$ = 2.098, g_{zz} = 2.484) characteristic of $3d^9$ configuration (Fig. 2b).

Adsorption of CO on the reduced sample resulted in a rhombic EPR signal (Fig. 2c) attributed to the Ni^I-CO monocarbonyl complexes. Only the spectrum registered for the lowest CO coverage is shown. For higher CO pressures, the EPR spectrum evolved progressively indicating a sequential formation of various polycarbonyl species [9]. The g-tensor parameters obtained via computer simulation are listed in Table 1. As compared to the Ni^I signal, the g-tensor changed not only its symmetry upon CO interaction but also the sequence of the

Table 1. Simulated EPR g-tensor components for the investigated nickel complexes with CO, NO, and O_2 molecules

Complex	g_{xx}	g_{yy}	g_{zz}
Ni^IZSM-5	2.098 ± 0.001	2.098 ± 0.001	2.478 ± 0.005
Ni^ICO/ZSM-5	2.016 ± 0.002	2.377 ± 0.005	2.432 ± 0.005
Ni^{II}NO/ZSM-5	2.155 ± 0.002 2.167 ± 0.002	2.212 ± 0.002 2.192 ± 0.002	2.357 ± 0.005 2.296 ± 0.005
$Ni^I O_2$/ZSM-5	2.062 ± 0.001 2.062 ± 0.001	2.086 ± 0.001 2.075 ± 0.001	2.164 ± 0.002 2.166 ± 0.002

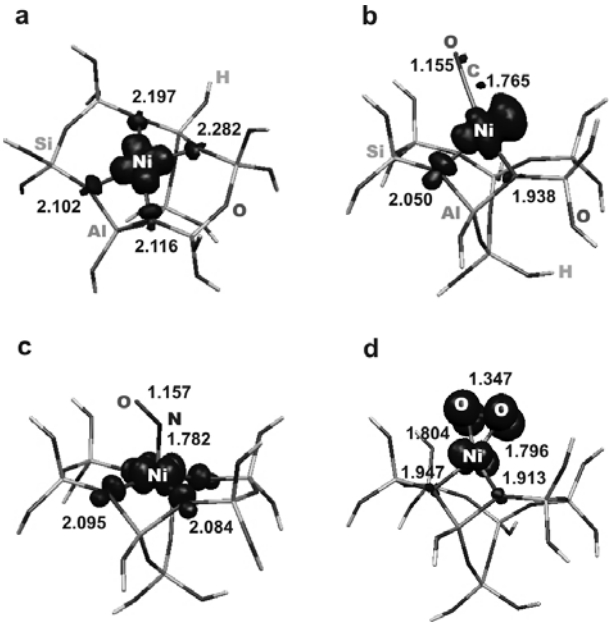

Fig. 3. BP/TZP optimized structures and the spin density contours of the (a) Ni^{I}/M7, (b) $Ni^{I}CO$/M7, (c) $Ni^{II}NO$/M7, and (d) $Ni^{I}O_2$/M7 models of adsorption complexes. M7 = $[Al_nSi_{7-n}O_8(OH)_{12}]$ (n = 1, 2) stands for a cluster mimicking the exchangeable site of the ZSM-5 zeolite. Bond lengths are given in angstroms.

g_{ii} components, suggesting strong rehybridization of the *d*-orbitals. Indeed, comparison of the DFT calculated spin density contours for the $Ni^{I}[AlSi_6O_8(OH)_{12}] \equiv Ni^{I}$/M7 cluster, mimicking the exchangeable sites of ZSM-5 zeolite, (Fig. 3a) and for the $Ni^{I}CO$/M7 cluster (Fig. 3b) showed a dramatic change in the nature of the singly occupied molecular orbital (SOMO) from the $d(x^2 - y^2)$ state to the $0.7 \times dxz + 0.3 \times (dxy + d(x^2 - y^2) + dz^2)$ state. The calculated *g*-tensor parameters for the $Ni^{I}CO$/M7 cluster were equal to $g_{xx} = 2.019$, $g_{yy} = 2.264$, and $g_{zz} = 2.428$, remaining in a reasonable agreement with the experimental values (Table 1). As compared to the four-coordinated planar Ni^{I} centre with the average Ni-O bond length of 2.174 Å, the nickel core is three-coordinated with only two Ni-O links (2.043 and 1.926 Å) and one shorter Ni-CO bond of 1.748 Å. The intramolecular C-O bond length equals 1.155 Å (Fig. 3b). The trigonal coordination assumes the so-called T-type geometry [1, 10] with the following schematic electron redistribution $[\uparrow Ni^{I}CO]^{+}$ ($\uparrow$ stands for the unpaired electron). A slight increase of the *g*-tensor anisotropy for the $Ni^{I}CO$ adduct with respect to the Ni^{I} could be related to the strong covalent interaction of the frontier CO orbitals (Fig. 1) with 3*d* orbitals of nickel resulting in a decreased splitting of the CO-Ni hybrids. According to the approximate perturbation formula for calculation of the *g*-tensor parameters [15]

$$\Delta g_{ij}^{p,m-n} \propto \frac{1}{2c(\varepsilon_n^{\sigma} - \varepsilon_m^{\sigma})} \left\langle \Psi_m^{\sigma} \middle| i L_{i=x,y,z} \middle| \Psi_n^{\sigma} \right\rangle \quad (3)$$

where Ψ_m and Ψ_n are the unperturbed Kohn-Sham orbitals, ε is the one-electron energy, L is the orbital momentum operator, whereas σ stands for the α or β spin, the higher the energy difference (greater splitting of the orbitals due to increased ligand field) the lower the *g*-tensor anisotropy.

The g_{zz} value (middle g_{ii} component) was shown to change monotonously with the tilt angle ∠N-Ni-C for the three-coordinate monocarbonyl diketiminate-Ni^{I} complexes following the simple equation [10]:

$$-b\ln[(g_{zz} - g_{180})/a] = \mathrm{tg}\alpha \quad (4)$$

where α stands for the N-Ni-C angle, $g_{180} = 2.133$ is a value of the g_{zz} for the $\alpha = 180°$ geometry, $a = 0.010$, and $b = 0.359$. Because the monocarbonyl diketiminate-Ni^{I} complex exhibits analogous type of the geometry as the $Ni^{I}CO$/M7 adducts (with nitrogen atoms replaced by oxygens), the above equation was used for discrimination between the Y- or T-geometries of the intrazeolitic nickel-carbonyl complex. Substituting the numerical value of the middle *g*-component 2.377 of the $Ni^{I}CO$/ZSM-5 species, the α tilt angle equal to 131° was obtained, which is indicative of the T-type geometry.

Interaction of NO with nickel(II)

The EPR spectrum of NO adsorption on the Ni^{II}/ZSM-5 zeolite is shown in Fig. 2d. Computer simulation revealed the presence of at least two component signals with the similar spin-Hamiltonian parameters given in Table 1. To get more insight into the electronic nature of the *g*-tensor of the $Ni^{II}NO$ adduct, a simple semi-empirical treatment developed originally for the O_2^- ($^2\Pi_{3/2}$) species by Känzing and Cohen [4] was used. In the free NO molecule the spin and the orbital magnetic moments are antiparallel and almost cancel each other. In this state NO is effectively nonmagnetic, and no EPR signal could be observed. This picture is strictly valid at low temperatures such as liquid helium, where occupation of the $\Pi_{3/2}$ state is negligible. At higher temperatures the EPR spectrum could be obtained in the gas phase because of the low lying excited $\Pi_{3/2}$ state. Upon removing the degeneracy of both π_g^* orbitals, $\pi_x^* = (1/\sqrt{2})(\pi_{-1}^* - \pi_1^*)$ and $\pi_y^* = (i/\sqrt{2})(\pi_{-1}^* + \pi_1^*)$, due to the interaction with the TMI centers, the orbital magnetic moment is quenched, and in such a case the unpaired electron is assumed to be localized on one of the π_g^* orbitals. The crystal field distortion $\Delta = \langle \pi_y^* | V_{CF} | \pi_y^* \rangle - \langle \pi_x^* | V_{CF} | \pi_x^* \rangle$ gives rise to two states with the energies equal to $\pm 1/2\lambda_0[1 + (\Delta/\lambda_0)^2]^{1/2}$, where $\lambda_0 = 123$ cm^{-1} (0.015 eV) is the free-molecule spin-orbit coupling constant. Taking into account second-order contribution due to the promotion of the electron from the σ orbital to the π^* (E), the following formulas for the *g*-tensor in terms of λ, Δ, and E parameters are obtained [2, 4]

$$\begin{aligned} g_{xx} &= g_e\cos 2\alpha - (\lambda/E)(1 - \sin 2\alpha - \cos 2\alpha) \\ g_{yy} &= g_e\cos 2\alpha - (\lambda/E)(\sin 2\alpha - \cos 2\alpha - 1) \\ g_{zz} &= g_e + 2l\sin 2\alpha \end{aligned} \quad (5)$$

where $\tan 2\alpha$ is defined as λ/Δ and $\lambda = i\langle \pi_y^* | L_z | \pi_x^* \rangle$. From these equations, it follows that $g_{yy} \sim g_{xx} < g_{zz}$, and the only important shift from g_e value is expected for the g_{zz} component. However, the experimentally observed signal for $Ni^{II}NO$ complex exhibited completely different parameters with a much pronounced *g*-tensor anisotropy. The shape and symmetry of the signal is similar to

Table 2. Calculated (BP/TZP-SOMF) EPR *g*-tensor components for various geometrical models of the O_2-nickel(I) complexes

Structure	g_{xx}	g_{yy}	g_{zz}
$[\eta^1\text{-}NiO_2(H_2O)_2]^+$	1.868	1.897	2.037
$[\eta^2\text{-}NiO_2(H_2O)_2]^+$	2.040	2.071	2.149
$[Ni\text{-}O(H_2O)_2]^+$	2.109	1.984	2.019
$[O\text{-}Ni\text{-}O(H_2O)_2]^+$	2.023	2.048	1.998
$\mu\text{-}Ni(\mu\text{-}1,2\text{-}O_2)Ni[(H_2O)_2OH]_2$	2.049	2.092	2.136
$[\mu\text{-}\eta^2\text{:}\eta^2\text{-}O_2Ni_2((H_2O)(OH))_2]^+$	2.138	2.059	2.040

that of bare Ni^I centres and the *g*-tensor parameters are characteristic of a metal-centred paramagnet with the $3d^9$ electron configuration [16]. Indeed, the calculated spin density contour for the $Ni^{II}NO$/M7 cluster (Fig. 3c) is similar to that of the Ni^I/M7 (Fig. 3a). As the bare nickel(II) centres exhibit triplet spin state, the nitrosyl adducts with spin doublet state are apparently formed via spin-pairing mechanism, accompanied by partial ligand-to-metal electron transfer (LMET) schematically described as $[\uparrow Ni^{II}\downarrow\uparrow NO]^{2+}$. The NO molecule is thereby transformed into the nitrosonium $NO^{\delta+}$ species upon ligation [11], leaving not appreciable spin density at the nitrogen nucleus, which results in the observed lack of the nitrogen hyperfine splitting in the EPR spectrum. The calculated coordination geometry of the resultant adduct exhibits a tetragonal pyramid with the NO ligand in the apical position (Fig. 3c). Four Ni-O bonds are relatively short (the average length of 2.106 Å is shorter than that obtained for the Ni^IM7 site), while the link between NO and nickel core equals 1.782 Å. The NO ligand is attached angularly (127°), and displays the intramolecular bond length of 1.157 Å.

Nickel-dioxygen adducts

Interaction of O_2 with nickel was investigated using the reduced Ni^I/ZSM-5 samples. The resultant EPR signal and its computer simulation are depicted in Fig. 2e. The simulation was carried out assuming two contributing species with slightly different *g*-tensor parameters (Table 1). They are characteristic of a superoxo radical O_2^- bound to the nickel(II) core [8]. In order to attribute the obtained experimental parameters to the plausible Ni-O_2 structures, a series of model molecular complexes were optimized and their *g*-tensor parameters were calculated. The coordination geometries included the cases of molecular adsorption (η^1-NiO_2 and η^2-NiO_2), dissociative adsorption (Ni-O and O-Ni-O) as well as attachment of O_2 as a bridging ligand (linear bridge $Ni(\mu\text{-}1,2\text{-}O_2)Ni$ and side bridge $\mu\text{-}\eta^2\text{:}\eta^2\text{-}(O_2Ni_2)$ species). The optimized structures are shown in Fig. 4 and their calculated *g*-tensor components are listed in Table 2. Comparison of the calculated and the experimental (Table 1) *g*-tensor values for the various investigated geometries of the Ni^I and O_2 interaction indicated that only the η^2-NiO_2 or $Ni(\mu\text{-}1,2\text{-}O_2)Ni$ species could be responsible for the observed EPR signal. Further calculations involving explicitly the zeolite environment (M7 cluster) confirmed that only the η^2-NiO_2/M7 cluster reproduces the experimental features. The geometry of this species and the spin density contour are shown in Fig. 3d. The spin density redistribution indicates that the superoxo radical is formed via metal to ligand electron transfer (MLET) resulting in the $[Ni^{II}\downarrow\uparrow O_2^-\uparrow]^+$ electronic structure. The η^2 coordination results in a trigonal geometry of the Ni-O_2 core (Ni-O_2 bonds equal to 1.804 and 1.796 Å), which, in turn, is bound to the zeolite by two additional Ni-O links (1.947 and 1.913 Å). The O-O bond in the O_2 moiety equals 1.347 Å and is 0.113 Å longer than that of the free O_2 molecule. This remains in agreement with reduction of dioxygen and formation of the superoxo O_2^- radicals. The BP/SOMF calculated *g*-tensor parameters for the η^2-NiO_2/M7 cluster are equal to g_{xx} = 2.039, g_{yy} = 2.098, and g_{zz} = 2.178, whereas those characteristic of the $Ni(\mu\text{-}1,2\text{-}O_2)$ Ni/M7-M5 cluster are equal to g_{xx} = 1.954, g_{yy} = 1.986, and g_{zz} = 2.080. Nice agreement of the calculated and the experimental counterparts observed for the η^2-NiO_2/M7 structure definitely proves the correct assignment of the superoxo-nickel geometry.

At first glance, the electronic nature of the experimental *g*-tensor of the η^2-NiO_2 complex can again be analyzed using the Känzing and Cohen model. For

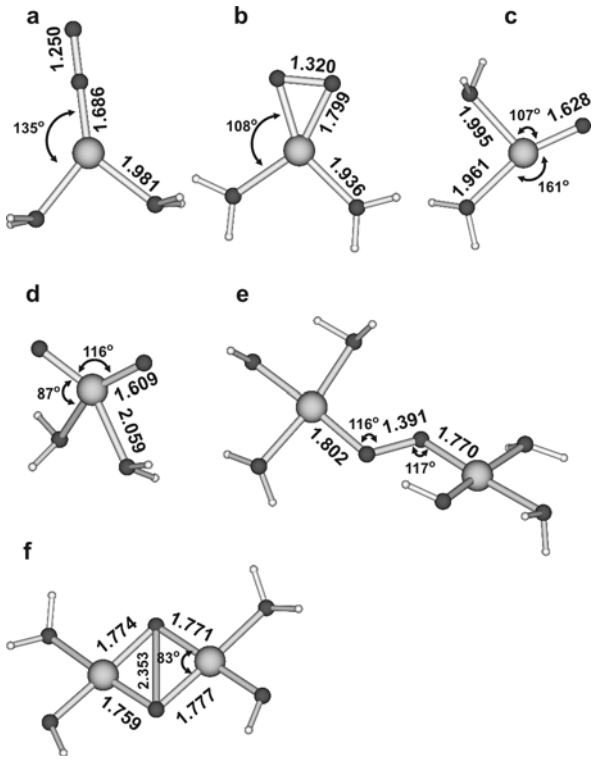

Fig. 4. BP/TZP optimized geometries of various possible molecular models of O_2-nickel(I) complexes: (a) $[\eta^1\text{-}NiO_2(H_2O)_2]^+$, (b) $[\eta^2\text{-}NiO_2(H_2O)_2]^+$, (c) $[Ni\text{-}O(H_2O)_2]^+$, (d) $[O\text{-}Ni\text{-}O(H_2O)_2]^+$, (e) $\mu\text{-}Ni(\mu\text{-}1,2\text{-}O_2)Ni[(H_2O)_2OH]_2$, (f) $[\mu\text{-}\eta^2\text{:}\eta^2\text{-}O_2Ni_2((H_2O)(OH))_2]^+$. Bond lengths are given in angstroms, and angles, in degrees.

the free superoxo radical O_2^- ($\sigma_g^2\pi_u^4\pi_g^{*3}$), the unpaired electron occupies two degenerate antibonding $\pi_g^*(2p)$ orbitals giving rise to the $^2\Pi_{3/2}$ ground state. The corresponding magnetic moment due to orbital and spin angular momenta is proportional to $L + g_eS$ and causes the *g*-tensor to be extremely anisotropic with $g_{||} = 2\langle+1, +1/2|\ L_z + 2S_z|\ +1, +1/2\rangle = 4$ and $g_\perp = \langle+1, -1/2|\ L_x + 2S_x|\ -1, +1/2\rangle = 0$. As a result, the powder-like spectrum of the superoxo radicals will extend over a large magnetic field, being too weak to be detected unless the orbital momentum is partially quenched due to the interaction with the environment. In such a case the unpaired electron is assumed to be localized in one of the $\pi_{(x,y)}^*{}_g$ orbitals, and the crystal field distortion Δ gives rise to two states with the energies equal to $\pm\ 1/2\lambda_0[1 + (\Delta/\lambda_0)^2]^{1/2}$, where $\lambda_0 = 0.014$ eV. From the Eqs. (5) it follows that $g_{zz} >> g_{yy} > g_{xx} \approx g_e$ and the biggest shift from g_e value is expected for the g_{zz} component. However, as compared to the η^2-{Ni^{II}-O_2^-} adduct in ZSM-5 the g_{ii} parameters are distinctly shifted toward higher values and they exhibit higher anisotropy. This is a direct consequence of the involvement into magnetic couplings the nickel-based states due to a relatively strong covalency of the Ni-O bonds [8].

Conclusions

Combination of EPR and DFT methods allowed for studying the interaction of CO, NO, and O_2 diatomic molecules with oxidized and reduced nickel ions inside the ZSM-5 zeolite. The corresponding adducts were identified and their structures ascertained by DFT geometry optimization and relativistic *g*-tensor calculations. It was found that CO binding resulted in trigonal coordination of the monocarbonyl adducts $[\uparrow Ni^{I}CO]^+$, leading to a profound change in the nature of the nickel-based SOMO. The nitrosyl adducts were formed via spin-pairing mechanism accompanied by partial LMET process, giving rise to the following magnetic structure $[\uparrow Ni^{II}\downarrow\uparrow NO]^{2+}$. It was found that upon ligation the bound NO molecule assumed an electrophilic $NO^{\delta+}$ character. In the case of the nickel-dioxygen complexes various possible modes of O_2 binding were explored and discriminated based on comparison of the calculated (BP/SOMF) *g*-tensor components with their experimental counterparts. Activation of O_2 occurred along the redox pathway, leading to dioxygen reduction via MLET and formation of the superoxo O_2^- species. The resulting adducts exhibited a mixed covalent-ionic $[Ni^{II}\downarrow\uparrow O_2^-\uparrow]^+$ electronic structure and the triangular η^2-NiO_2 geometry.

Acknowledgment. This work was supported by the Ministry of Science and Higher Education (MNiSW) of Poland under research project IP2011 041871. T. Mazur thanks for the support from the International PhD-studies at the Faculty of Chemistry, Jagiellonian University, within the MPD Programme of the Foundation for Polish Science co-financed by the EU Regional Development Fund. K. Podolska thanks for the postdoc position from the SET project at the Jagiellonian University. The research was carried out with the equipment purchased thanks to the financial support of the EU Regional Development Fund in the framework of the Polish Operational Programme – Innovative Economy (contract no. POIG.02.01.00-12-023/08).

References

1. Harrop TC, Olmstead MM, Mascharak PK (2006) Synthetic analogues of the active site of the A-cluster of acetyl coenzyme A synthase/CO dehydrogenase: syntheses, structures, and reactions with CO. Inorg Chem 45:3424–3436
2. Hoffman BM, Nelson NJ (1969) Structure of nitric oxide adsorbed on 4A molecular sieve. J Chem Phys 50:2598–2603
3. http://thch.uni-bonn.de/tc/orca
4. Känzig W, Cohen MH (1959) Paramagnetic resonance of oxygen in alkali halides. Phys Rev Lett 3:509–510
5. Kubas GJ (2007) Fundamentals of H_2 binding and reactivity on transition metals underlying hydrogenase function and H_2 production and storage. Chem Rev 107:4152–4205
6. Mosqueda-Jiménez BI, Jentys A, Seshan K, Lercher JA (2003) Structure-activity relations for Ni-containing zeolites during NO reduction II. Role of the chemical state of Ni. J Catal 218:375–385
7. Neese F (2005) Efficient and accurate approximations to the molecular spin-orbit coupling operator and their use in molecular *g*-tensor calculations. J Chem Phys 122:034107
8. Pietrzyk P, Podolska K, Mazur T, Sojka Z (2011) Heterogeneous binding of dioxygen: EPR and DFT evidence for side-on nickel(II)-superoxo adduct with unprecedented magnetic structure hosted in MFI zeolite. J Am Chem Soc 133:19931–19943
9. Pietrzyk P, Podolska K, Sojka Z (2008) DFT analysis of *g* and ^{13}C hyperfine coupling tensors for model $Ni^{I}(CO)_nL_m$ ($n = 1 \div 4$, L = H_2O, OH^-) complexes epitomizing surface nickel(I) carbonyls. J Phys Chem A 112:12208–12219
10. Pietrzyk P, Podolska K, Sojka Z (2009) Resolving conformation dichotomy for Y- and T-shaped three-coordinate Ni^{I} carbonyl complexes with relativistic DFT analysis of EPR fingerprints. Chem Eur J 15:11802–11807
11. Pietrzyk P, Podolska K, Sojka Z (2011) Role of $NO^{\delta+}$ intermediates in NO reduction with propene over NiZSM-5 zeolite revealed by EPR and IR spectroscopic investigations and DFT modeling. J Phys Chem C 115:13008–13015
12. Pietrzyk P, Podolska K, Sojka Z (2012) Molecular interpretation of EPR parameters – computational spectroscopy approaches. Electron Paramag Reson 23:264–311
13. Pietrzyk P, Sojka Z (2007) Co^{2+}/Co^0 redox couple revealed by EPR spectroscopy triggers preferential coordination of reactants during SCR of NO_x with propene over cobalt-exchanged zeolites. Chem Commun 19:1930–1932
14. Sadło J, Michalik J, Kevan L (2006) EPR and ESEEM study of silver clusters in ZK-4 molecular sieves. Nukleonika 51;Suppl 1:S49–S54
15. Schreckenbach G, Ziegler T (1997) Calculation of the *g*-tensor of electron paramagnetic resonance spectroscopy using gauge-including atomic orbitals and density functional theory. J Phys Chem A 101:3388–3399
16. Sojka Z, Pietrzyk P, Martra G, Kermarec M, Che M (2006) EPR and DFT study of NO interaction with Ni/SiO_2 catalyst: insight into mechanistic steps of disproportionation process promoted by tripodal surface nickel complex. Catal Today 114:154–161
17. Spalek T, Pietrzyk P, Sojka Z (2005) Application of genetic algorithm joint with Powell method to non-linear least-squares fitting of powder EPR spectra. J Chem Inf Model 45:18–29

18. te Velde G, Bickelhaupt FM, Baerends EJ *et al*. (2001) Chemistry with ADF. J Comput Chem 22:931–967

19. Yao S, Driess M (2012) Lessons from isolable nickel(I) precursor complexes for small molecule activation. Acc Chem Res 45:276–287